Precambrian Research 236 (2013) 182–192

Contents lists available at ScienceDirect

Precambrian Research

journal homepage: www.elsevier.com/locate/precamres

Geochemical, Sr–Nd isotopic, and zircon U–Pb geochronological constraints on the petrogenesis of Late Paleoproterozoic mafic dykes within the northern North China Craton, Shanxi Province, China

Shen Liu[a,c,*], Caixia Feng[a,c], Bor-ming Jahn[b], Ruizhong Hu[c], Shan Gao[d], Guangying Feng[e], Shaocong Lai[a], Yuhong Yang[c], Youqiang Qi[c], Ian M. Coulson[f]

[a] State Key Laboratory of Continental Dynamics and Department of Geology, Northwest University, Xi'an 710069, China
[b] Department of Geosciences, National Taiwan University, Taipei, Taiwan
[c] State Key Laboratory of Ore Deposit Geochemistry, Institute of Geochemistry, Chinese Academy of Sciences, Guiyang 550002, China
[d] State Key Laboratory of Geological Processes and Mineral Resources, China University of Geosciences, Wuhan 430074, China
[e] Institute of Geology, Chinese Academy of Geological Sciences, Beijing 100037, China
[f] Solid Earth Studies Laboratory, Department of Geology, University of Regina, Regina, Saskatchewan S4S 0A2, Canada

ARTICLE INFO

Article history:
Received 29 March 2013
Received in revised form 9 July 2013
Accepted 10 July 2013
Available online 8 August 2013

Keywords:
Paleoproterozoic
Mafic dykes
Origin
Extension
Northern NCC

ABSTRACT

The ages and source of Precambrian mafic dolerite dykes of the North China Craton (NCC) were determined using geochronological, geochemical, and whole-rock Sr–Nd isotopic data. Laser ablation–inductively coupled plasma-mass spectrometry (LA–ICP-MS) U–Pb analysis of zircons yielded consistent ages of 1621 ± 6 and 1621 ± 7 Ma for two mafic dykes (SYG01 and SYG02) within the NCC. The dykes are classified as the sub-alkaline series according to their $K_2O + Na_2O$ concentrations (2.5–2.9 wt%), and as the calc-alkaline series according to their K_2O concentrations (0.05–0.72 wt%). These dykes also contain low concentrations of the light rare earth elements [$(La/Yb)_N$ = 1.5–2.4], with negligible Eu anomalies (δEu = 0.9–1.1), positive Ba, Pb, and K anomalies, and depletions in Th, U, and high field strength elements (P and Ti). In addition, the dykes contain relatively low amounts of radiogenic Sr[$(^{87}Sr/^{86}Sr)_i$ = 0.7025–0.7035] and have high $\varepsilon_{Nd}(t)$ values (5.6–5.8). These data suggest that the dykes were derived from a depleted mantle source that was hybridized during interaction with foundered lower crustal material. The parental mafic magmas underwent the fractionation of olivine, pyroxene, hornblende, and Fe–Ti oxides (e.g. rutile, ilmenite, titanite) during ascent, with negligible evidence for crustal contamination prior to emplacement at a high crustal level. The NCC extension was related to foundering of lower crust, and there were three episodes of lithosphere extension during Proterozoic time (i.e. 1.8–1.6 Ga, 1.3–1.2 Ga, and 0.8–0.7 Ga).

1. Introduction

The fact that mafic dykes may be emplaced as a result of lithospheric-scale extension (Halls, 1982; Féraud et al., 1987; Halls and Fahrig, 1987; Tarney and Weaver, 1987; Zhao and McCulloch, 1993; Gudmunsson, 1995) suggests that mafic dyke swarms can provide valuable information on the processes involved in the generation of voluminous mafic magmas. In addition, such dykes can provide insight into lithospheric and tectonic processes, including extension, crust–mantle interaction, and the sourcing of magmas during breakup of cratons (Liu et al., 2005, 2006, 2008a,b, 2009, 2012a,b, 2013). Furthermore, mafic dyke swarms are commonly related to significant precious and base metal mineralization, which has led to many studies of mafic dykes worldwide and to the relationship of these important magmas to ore-genesis.

Important swarms of mafic dykes are located in and across North America, Brazil, the area around the Baltic Sea, Australia, South Africa, Scotland, and the Tibet and Tarim provinces of South and North China. The occurrence frequency of mafic dyke magmatism shows peaks at 2.4, 2.1, 1.8, 1.4, 1.0 Ga, and 230–40 Ma (Liu et al., 2010a,b). Of particular note are the more than 600 mafic dykes that have been identified within the North China Craton (NCC); these dykes have been the focus of a significant body of research (e.g. Chen and Shi, 1983, 1994; Chen et al., 1992; Shao and Zhang, 2002; Zhang and Sun, 2002; Shao and Zhang, 2002; Shao et al., 2003; Zhai et al., 2003, 2004; Xu, 2004; Yang et al., 2004; Liu et al., 2005, 2006, 2008a,b, 2009, 2012b; Liu et al., 2013; Peng et al., 2005, 2007, 2008, 2010, 2011a,b; Hou et al., 2006; Yan et al., 2007; Wang et al., 2007;

* Corresponding author at: State Key Laboratory of Continental Dynamics and Department of Geology, Northwest University, Xi'an 710069, China.
Tel.: +86 29 88300226; fax: +86 29 88300226.
E-mail addresses: liushen@vip.gyig.ac.cn, liushen@nwu.edu.cn (S. Liu).

0301-9268/$ – see front matter © 2013 Elsevier B.V. All rights reserved.
http://dx.doi.org/10.1016/j.precamres.2013.07.007

Lin et al., 2008a; Lu et al., 2008; Wu et al., 2008; Zhang, 2009; John et al., 2010; Li et al., 2010; Peng, 2010). Nevertheless, controversy over the processes involved in the destruction of the NCC has meant that the majority of research has focused on Mesozoic and Cenozoic mafic dykes of the Craton, and little attention has been paid to Precambrian lithospheric extension within the NCC, which requires geochronological, geochemical, and isotopic characterization of the Precambrian mafic dykes of the Craton. In this paper, we present new laser ablation–inductively coupled plasma-mass spectrometry (LA–ICP-MS) zircon U–Pb, petrological, whole-rock geochemical, and Sr–Nd isotopic data for representative mafic dykes samples from the northern NCC within the Shanxi Province. These data allow us to constrain the emplacement ages and origin of these dykes.

2. Geological setting and petrography

The NCC is located in eastern China, covering a wide area ($\sim 170 \times 10^4$ km^2; Wu et al., 2008), and consists of the Archean Eastern and Western Blocks, which collided along the nearly N–S-trending Paleoproterozoic Trans-North China Orogen at ~1.85 Ga (Fig. 1; Zhao et al., 2001, 2005; Wilde et al., 2002; Guo et al., 2005). The Eastern and Western Blocks can be further divided into microcontinental blocks and active belts (Zhai and Bian, 2000; Zhao, 2009). For example, the Western Block consists of the Yinshan Block in the north and the Ordos Block in the south, separated by the E–W-trending paleoproterozoic Khondalite Belt (Fig. 1; Xia et al., 2008; Yin et al., 2009, 2011; Li et al., 2011; Wang et al., 2011), whereas the Eastern Block consists of the Longgang Block (also called the Yanliao Block) and the Langrim Block, separated by the Paleoproterozoic Jiao-Liao-Ji Belt (Fig. 1; Li et al., 2006; Luo et al., 2008; Li and Zhao, 2007; Zhou et al., 2008; Wang et al., 2009; Huang et al., 2009; Tam et al., 2011, 2012a,b; Zhao et al., 2010, 2012; Zhai, 2012; Zhao and Zhai, 2013; Wu et al., 2013a,b). As one of the oldest continents (Lin et al., 2008b), the NCC has a significant crustal age (>3.8 Ga; Liu et al., 1992; Zheng et al., 2005), whose southern and northern margin are the Indosinian Qingling-Dabie and Hercynian Yinshan-Yanshan Orogenic Belts, whereas the western margin is the Helanshan-Qilian Orogenic Belt and the eastern margin lies Korea. Traditionally, this area has been considered to be composed of uniform Precambrian (Archean-Sinian) crystalline basement, overlain by younger cover (Cambrian-Quaternary multiple types of rocks), and its tectonic history was explained using a pre-plate tectonic, geosynclinal-style model (Zhao et al., 2001). However, the regions with the most complete records are found in northern NCC (e.g. Shanxi and Hebei provinces, and Inner Mongolia), including Archean and paleoproterozoic basement (e.g. Hohhot, Datong, and Zhangjiakou), late mesoproterozoic rifts (e.g. Bayan Obo and Chengde) and epicontinental active belts (e.g. Duolun and Chifeng).

To date, more than 80 Precambrian mafic dykes with ages ranging from 2.5 to 0.8 Ga have been discovered in the NCC (Peng, 2010). The present study focuses on mafic dolerite dykes that intruded into Archean diorite in the Shangyaogou area of northern Shanxi Province (samples SYG-1 to SYG-16), in northern NCC. These dykes (Table 2 and Fig. 1b and 2) are vertical, trending along a NE–SW belt that extends between 50 m and 2.5 km wide, and 12–15 km long (Fig. 1b). Representative photomicrographs of mafic dyke lithologies within the Shangyaogou area are shown in Fig. 2. These dykes are dominated by dolerites, with typical dolerite/diabase textures, and contain medium-grained clinopyroxene (2.0–6.0 mm) and lath-shaped plagioclase (2.5–5.0 mm) phenocrysts within a matrix (60–65% of the rock mass) of clinopyroxene (0.05–0.06 mm), plagioclase (0.02–0.05 mm), minor magnetite (~0.02–0.04 mm) and chlorite (0.04–0.06 mm), and accessory zircon and apatite.

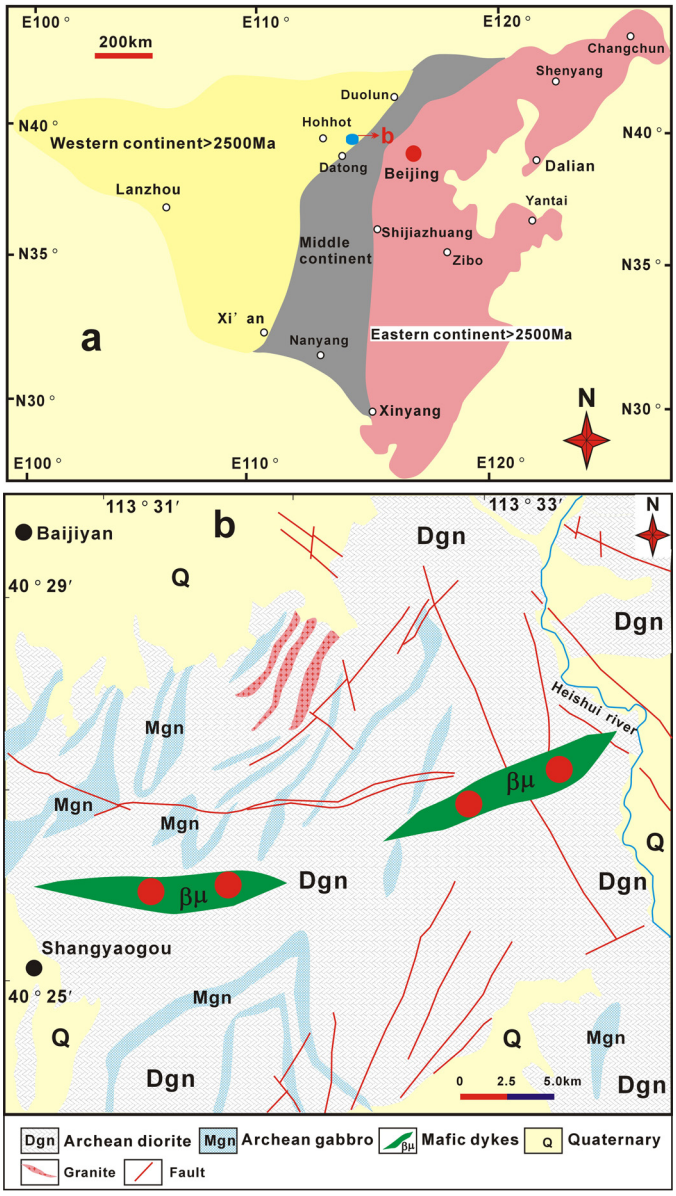

Fig. 1. (a) Location of the study area in China. (b) Geological maps of the study area, showing the distribution of mafic dykes and sampling localities.

3. Analytical techniques

3.1. Zircon LA–ICP-MS U–Pb dating

Zircons were separated from two samples (SYG01 and SYG02) using conventional heavy liquid and magnetic techniques at the Langfang Regional Geological Survey, Hebei Province, China. After separation and mounting, the internal and external structures of the zircon grains were imaged using transmitted and reflected light, and by cathodoluminescence (CL) techniques at the State Key Laboratory of Continental Dynamics, Northwest University, Xi'an, China. Prior to zircon U–Pb dating, grain mount surfaces were washed in dilute HNO_3 and pure alcohol to remove any potential lead contamination. Zircon U–Pb ages were determined by LA–ICP-MS (Table 1 and Fig. 3) using an Agilent 7500a ICP-MS instrument equipped with a 193 nm excimer laser at the State Key Laboratory of Geological Processes and Mineral Resources, China University of Geoscience, Wuhan, China. The #91500 zircon standard was used for quality control, and a NIST 610 standard was used for data

Table 1
LA–ICP-MS U–Pb isotope data for zircons from mafic dykes of the NCC.

Spot	Th (ppm)	U (ppm)	Pb (ppm)	Th/U	Isotopic ratios						Age (Ma)					
					$^{207}Pb/^{206}Pb$	1σ	$^{207}Pb/^{235}U$	1σ	$^{206}Pb/^{238}U$	1σ	$^{207}Pb/^{206}Pb$	1σ	$^{207}Pb/^{235}U$	1σ	$^{206}Pb/^{238}U$	1σ
SYG01																
1.1	79.6	92.4	35.3	0.86	0.0848	0.0018	3.8286	0.0714	0.2858	0.0015	1310	24	1599	16	1621	13
2.1	113	88.3	28.5	1.28	0.0983	0.0023	3.8273	0.0683	0.2863	0.0016	1592	23	1599	15	1623	12
3.1	205	166	58.7	1.23	0.1006	0.0027	3.9035	0.7286	0.2853	0.0013	1635	362	1614	151	1618	12
4.1	114	141	38.2	0.81	0.0988	0.0023	3.9171	0.0716	0.2855	0.0016	1602	23	1617	15	1619	11
5.1	243	192	52.3	1.27	0.1005	0.0013	3.9155	0.0694	0.2864	0.0015	1633	20	1617	14	1624	13
6.1	87.5	92.4	41.4	0.95	0.1007	0.0017	3.9166	0.0679	0.2863	0.0013	1637	21	1617	14	1623	11
7.1	162	223	75.1	0.73	0.1003	0.0018	3.9162	0.0709	0.2861	0.0015	1630	25	1617	15	1625	10
8.1	139	215	81.7	0.65	0.0985	0.0024	3.8175	0.0717	0.2862	0.0014	1596	32	1412	18	1623	12
9.1	133	62.6	34.4	2.12	0.1006	0.0022	3.9178	0.0712	0.2856	0.0016	1635	24	1617	15	1620	9
10.1	182	108	36.8	1.69	0.0992	0.0022	3.9159	0.0681	0.2853	0.0015	1609	20	1617	14	1618	13
11.1	137	157	64.8	0.87	0.0987	0.0018	3.9164	0.0679	0.2851	0.0016	1600	23	1617	14	1617	9
12.1	121	113	51.5	1.07	0.1002	0.0025	3.9181	0.0681	0.2861	0.0014	1628	20	1617	14	1622	12
SYG02																
1.1	89	93	34.6	0.95	0.0848	0.0018	3.8286	0.0744	0.2858	0.0016	1310	24	1599	16	1621	13
2.1	123	89.5	29.2	1.37	0.0983	0.0023	3.8273	0.0731	0.2863	0.0014	1592	23	1599	15	1623	12
3.1	208	173	57.6	1.20	0.1006	0.0027	3.9035	0.7286	0.2853	0.0013	1635	362	1614	151	1618	12
4.1	116	145	41.3	0.80	0.0988	0.0023	3.9171	0.0716	0.2855	0.0012	1602	23	1617	15	1619	11
5.1	237	203.0	51.6	1.17	0.1005	0.0013	3.9155	0.0694	0.2864	0.0015	1633	20	1617	14	1624	13
6.1	88.3	91.5	42.2	0.97	0.1007	0.0017	3.9166	0.0679	0.2863	0.0012	1637	21	1617	14	1623	11
7.1	164	218	74.8	0.75	0.1003	0.0018	3.9162	0.0729	0.2866	0.0014	1630	25	1617	15	1625	10
8.1	142	211	82.3	0.67	0.0985	0.0024	3.0175	0.0717	0.2862	0.0014	1596	32	1412	18	1623	12
9.1	135	62	33.2	2.19	0.1006	0.0022	3.9178	0.0712	0.2856	0.0015	1635	24	1617	15	1620	9
10.1	175.0	113	37.1	1.55	0.0992	0.0022	3.9159	0.0681	0.2853	0.0013	1609	20	1617	14	1618	13

optimization. A spot diameter of 24 μm was used during the analysis, employing the methodologies described by Yuan et al. (2004) and Liu et al. (2010a,b). Common Pb correction was undertaken following Andersen (2002), and the resulting data were processed using the GLITTER and ISOPLOT programs (Ludwig, 2003; Table 1 and Fig. 3). Uncertainties on individual LA–ICP-MS analyses are quoted at the 95% (1σ) confidence level.

3.2. Whole-rock geochemistry

The whole-rock and Sr–Nd isotope geochemical compositions of 16 samples were determined during this study. Prior to whole-rock geochemical analysis, samples were trimmed to remove altered surfaces, cleaned with de-ionized water, and crushed and powdered in an agate mill. Major element concentrations were determined on fused glass discs using a PANalytical Axios-advance (Axios PW4400) X-ray fluorescence spectrometer (XRF) at the State Key Laboratory of Ore Deposit Geochemistry, Institute of Geochemistry, Chinese Academy of Sciences, Guiyang, China. These analyses have a precision of better than 5%, as determined using the GSR-1 and GSR-3 Chinese National standards (Table 2). Loss on ignition (LOI) values were obtained using 1 g of powder heated to 1100 °C for 1 h. Trace element concentrations were determined using ICP-MS at the State Key Laboratory of Ore Deposit Geochemistry, Institute of Geochemistry, Chinese Academy of Sciences, Guiyang, following Qi et al. (2000). Triplicate analyses were reproducible to within 5% for all elements, and analyses of the OU-6 and GBPG-1 international standards agreed with recommended values (Table 3).

3.3. Sr–Nd isotope analyses

Sample powders used for Rb–Sr and Sm–Nd isotope analysis were spiked with mixed isotope tracers, dissolved in Teflon capsules using HF and HNO_3 acids, and separated by conventional cation-exchange techniques. Isotopic measurements were performed using a Finnigan Triton Ti thermal ionization mass spectrometer at the State Key Laboratory of Geological Processes and Mineral Resources, China University of Geosciences. Procedural blanks yielded concentrations of <200 pg for Sm and Nd, and <500 pg for Rb and Sr. Mass fractionation corrections for Sr and Nd isotopic ratios were based on $^{86}Sr/^{88}Sr = 0.1194$ and $^{146}Nd/^{144}Nd = 0.7219$, respectively, and analysis of the NBS987 and La Jolla standards yielded values of $^{87}Sr/^{86}Sr = 0.710246 \pm 16$ (2σ), and $^{143}Nd/^{144}Nd = 0.511863 \pm 8$ (2σ), respectively.

4. Results

4.1. Zircon U–Pb ages

Euhedral zircons in samples SYG01 and SYG02 are clean and prismatic, and contain oscillatory magmatic zoning (Fig. 3). Twelve zircons from sample SYG01 yielded a weighted mean $^{206}Pb/^{238}U$ age of 1621 ± 6 Ma (1σ, 95% confidence interval; Table 1 and Fig. 3a), with 10 zircons from sample SYG02 yielding a weighted mean $^{206}Pb/^{238}U$ age of 1621 ± 7 Ma (1σ; 95% confidence interval; Table 1 and Fig. 3b). These new data provide the best estimates of the crystallization ages of mafic dykes within the Shangyaogou area, and no inherited zircons were observed in either sample population.

4.2. Major and trace element geochemistry

The whole-rock geochemical compositions of mafic dykes sampled during this study are listed in Tables 2 and 3.

With the exception of two variable major elements ($K_2O = 0.05–0.72$ wt%, and $P_2O_5 = 0.05–0.15$ wt%), the mafic dykes have relatively uniform compositions, with $SiO_2 = 47.85–50.08$ wt%, $TiO_2 = 0.69–2.06$ wt%, $Al_2O_3 = 12.82–14.15$ wt%, $Fe_2O_3 = 13.49–18.03$ wt%, MnO = 0.18–0.25 wt%, MgO = 5.82–7.36 wt%, CaO = 9.51–10.94 wt%, and $Na_2O = 1.95–2.84$ wt%. All of these mafic dykes are classified as sub-alkaline on the total alkali-silica (TAS) diagram (Fig. 4a) and calc-alkaline in a Na_2O vs. K_2O diagram (Fig. 4b). These dykes have negative correlations between MgO and each of SiO_2, TiO_2, Fe_2O_3, MnO, and P_2O_5 concentrations (Fig. 5a, b, d, e and h), and are light rare earth element (LREE)-enriched and heavy rare earth element (HREE)-depleted, with a small range in $(La/Yb)_N$ (1.5–2.4) and Eu/Eu* (0.9–1.1) values (Table 3 and Fig. 6a). The dykes can also be split into two suites (Fig. 6a), both

Table 2
Major element concentrations (wt%) for mafic dykes of the NCC. LOI = loss on ignition, $Mg^{\#} = 100 \times Mg/(Mg + Fe)$ in atomic proportions, RV = recommended values, MV = measured values. Values for GSR-1 and GSR-3 are from Wang et al. (2003).

Sample	Rock type	SiO_2	TiO_2	Al_2O_3	Fe_2O_3	MnO	MgO	CaO	Na_2O	K_2O	P_2O_5	LOI	Total	$Mg^{\#}$
SYG-1	Dolerite	48.48	2.06	12.87	18.03	0.25	5.93	9.64	1.97	0.56	0.15	0.86	100.8	42
SYG-2	Dolerite	48.56	2.03	12.91	18.01	0.23	5.87	9.58	1.95	0.55	0.13	0.62	100.44	42
SYG-3	Dolerite	48.73	2.01	12.84	17.86	0.23	5.82	9.51	1.96	0.43	0.12	0.44	99.95	42
SYG-4	Dolerite	47.85	1.62	12.82	16.84	0.25	6.27	9.73	2.06	0.68	0.13	0.97	99.22	45
SYG-5	Dolerite	49.15	0.82	14.13	13.65	0.22	7.32	10.92	2.86	0.05	0.07	0.56	99.75	54
SYG-6	Dolerite	49.13	0.83	14.15	13.62	0.21	7.35	10.94	2.83	0.06	0.06	0.53	99.71	54
SYG-7	Dolerite	50.05	0.78	13.87	13.54	0.23	7.32	10.86	2.78	0.07	0.05	0.52	100.07	54
SYG-8	Dolerite	50.03	0.81	13.85	13.57	0.22	7.34	10.88	2.75	0.06	0.06	0.39	99.96	54
SYG-9	Dolerite	50.07	0.73	13.84	13.52	0.21	7.33	10.84	2.73	0.05	0.07	0.58	99.97	54
SYG-10	Dolerite	50.08	0.69	13.85	13.49	0.23	7.35	10.89	2.75	0.06	0.07	0.46	99.92	55
SYG-11	Dolerite	50.08	0.72	13.82	13.51	0.21	7.32	10.83	2.72	0.05	0.06	0.42	99.74	54
SYG-12	Dolerite	49.16	0.82	14.13	13.63	0.22	7.34	10.94	2.83	0.05	0.06	0.61	99.79	54
SYG-13	Dolerite	47.93	1.63	12.84	16.79	0.24	6.25	9.68	2.04	0.72	0.13	0.98	99.23	45
SYG-14	Dolerite	48.54	2.04	12.93	17.87	0.21	5.86	9.55	1.96	0.53	0.14	0.63	100.1118	42
SYG-15	Dolerite	49.19	0.79	14.12	13.61	0.21	7.36	10.86	2.84	0.06	0.06	0.62	100.332	54
SYG-16	Dolerite	50.06	0.71	13.85	13.51	0.18	7.35	10.76	2.72	0.06	0.07	0.66	100.1586	54
GSR-3	RV*	44.64	2.37	13.83	13.4	0.17	7.77	8.81	3.38	2.32	0.95	2.24	99.88	
GSR-3	MV*	44.75	2.36	14.14	13.35	0.16	7.74	8.82	3.18	2.3	0.97	2.12	99.89	
GSR-1	RV*	72.83	0.29	13.4	2.14	0.06	0.42	1.55	3.13	5.01	0.09	0.7	99.62	
GSR-1	MV*	72.65	0.29	13.52	2.18	0.06	0.46	1.56	3.15	5.03	0.11	0.69	99.70	

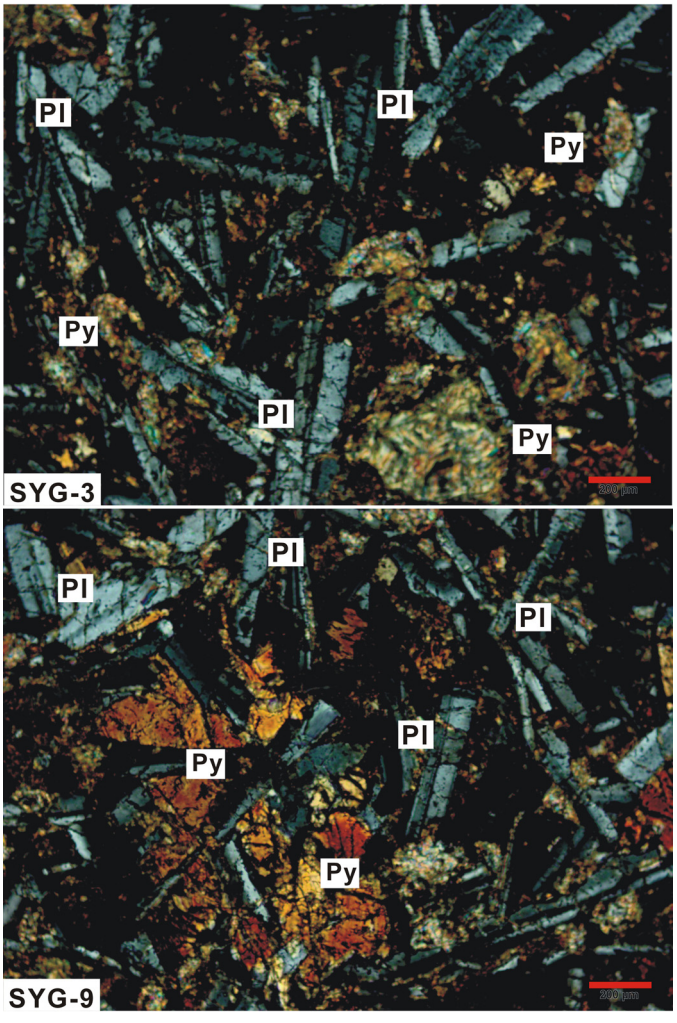

Fig. 2. Representative photomicrographs of mafic dykes from the northern NCC, China; all samples have doleritic textures and hence are termed dolerite dykes. Py, pyroxene; Pl, plagioclase.

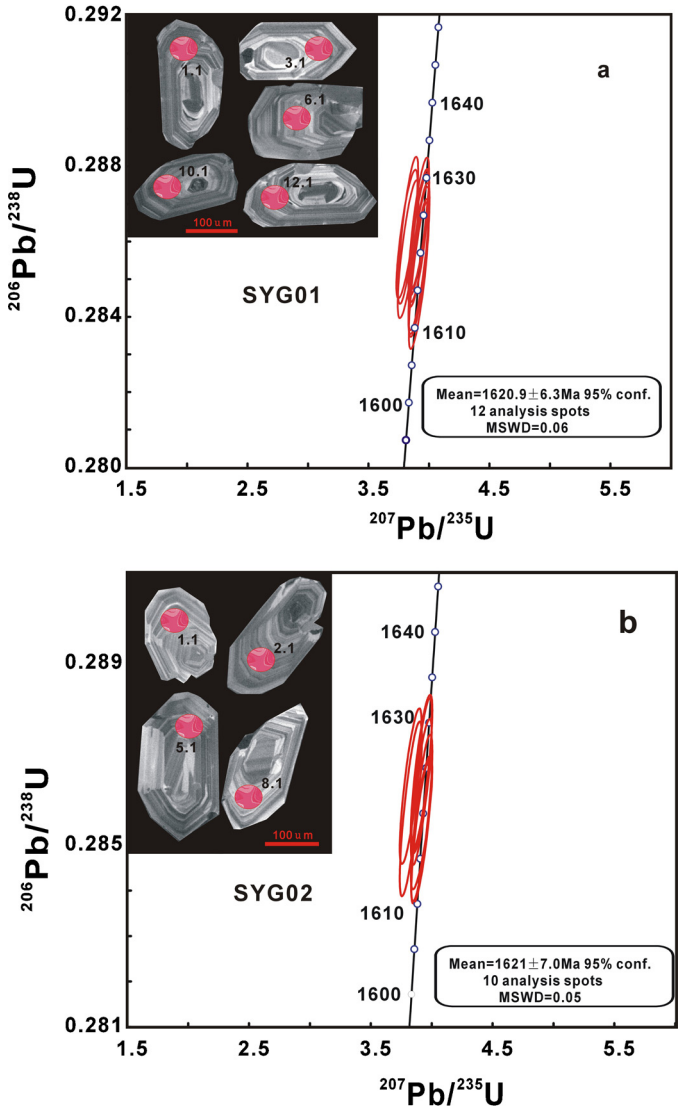

Fig. 3. Zircon LA–ICP-MS U–Pb concordia diagrams and CL images of zircons separated from mafic dykes within the northern NCC, China.

Table 3
Trace element compositions (in ppm) of mafic dykes within the NCC. Values for GBPG-1 and OU-6 are from Thompson et al. (2000) and Potts and Kane (2005), respectively.

Sample	SYG-1	SYG-2	SYG-3	SYG-4	SYG-5	SYG-6	SYG-7	SYG-8	SYG-9	SYG-10	SYG-11	SYG-12	SYG-13	SYG-14	SYG-15	SYG-16	OU-6 (RV*)	OU-6 (MV*)	GBPG-1 (RV*)	GBPG-1 (MV*)
Cr	123	126	118	128	131	134	146	137	125	136	135	143	141	116	127	145	70.8	73.5	181	187
Ni	65.3	61.3	56.7	61.1	66.9	72.1	71.2	71.8	61.5	72.6	72.4	72.3	71.8	57.3	61.3	71.8	39.8	42.5	59.6	60.6
Rb	18.2	7.82	5.36	7.82	15.3	14.9	12.5	15.2	7.85	15.4	14.6	23.1	13.3	5.35	7.84	22.2	120	122	56.2	61.4
Sr	141	144	146	147	175	183	143	185	146	182	186	141	145	153	143	152	131	136	364	377
Y	37.4	20.2	20.3	20.2	20.6	21.3	34.2	21.2	20.4	21.3	21.4	34.3	33.7	20.5	20.5	34.6	27.35	26.2	18.0	17.2
Zr	119	23.9	23.9	23.8	41.6	42.1	108	42.3	24.2	42.1	41.9	105	108	24.3	23.5	108	174	183	232	224
Nb	6.57	2.75	2.57	2.83	2.66	2.65	5.54	2.62	2.83	2.64	2.63	5.56	5.46	2.45	2.85	5.62	14.8	15.3	9.93	8.74
Ba	209	93.7	98.2	93.9	158	156	465	158	94.3	156	158	472	478	103	94.6	474	477	486	908	921
La	12.2	5.42	4.63	5.41	4.82	4.76	10.3	4.71	5.44	4.73	4.82	10.1	10.5	4.72	5.38	11.2	33	33.1	53.0	51.0
Ce	25.4	11.4	10.4	11.5	10.3	10.4	23.5	10.2	11.5	10.4	11.3	24.1	23.6	11.2	12.2	25.2	74.4	78.0	103	105
Pr	3.97	1.84	1.67	1.85	1.75	1.74	3.56	1.75	1.85	1.74	1.75	3.53	3.54	1.71	1.83	3.47	7.8	8.09	11.5	11.6
Nd	17.4	8.03	7.19	8.05	7.63	7.65	16.3	8.63	8.05	8.62	7.63	17.2	16.8	7.23	8.03	17.4	29.0	30.6	43.3	42.4
Sm	5.4	2.38	2.25	2.43	2.55	2.63	4.85	2.65	2.35	2.64	2.67	4.92	4.95	2.24	2.42	4.87	5.92	5.99	6.79	6.63
Eu	1.73	1.03	1.03	1.03	1.06	1.08	1.62	1.09	1.06	1.08	1.06	1.58	1.63	1.04	1.04	1.55	1.36	1.35	1.79	1.69
Gd	6.34	3.74	3.63	3.75	3.66	3.58	5.83	3.55	3.76	3.48	3.53	5.82	5.86	3.65	3.78	5.85	5.27	5.50	4.74	4.47
Tb	1.05	0.59	0.49	0.58	0.54	0.52	0.93	0.47	0.57	0.49	0.48	0.91	0.93	0.48	0.59	0.93	0.85	0.83	0.60	0.59
Dy	7.26	3.96	3.65	3.94	3.88	3.86	6.45	3.87	3.93	3.88	3.79	6.42	6.47	3.71	3.98	6.45	4.99	5.06	3.26	3.17
Ho	1.52	0.92	0.79	0.86	0.92	0.93	1.31	0.95	0.93	0.96	0.94	1.26	1.25	0.82	0.89	1.27	1.01	1.02	0.69	0.66
Er	4.32	2.61	2.52	2.53	2.54	2.62	3.83	2.63	2.62	2.66	2.63	3.81	3.93	2.53	2.54	3.93	2.98	3.07	2.01	2.02
Tm	0.57	0.29	0.31	0.28	0.32	0.31	0.56	0.32	0.28	0.33	0.2929	0.55	0.59	0.32	0.26	0.61	0.44	0.45	0.30	0.29
Yb	3.41	2.37	2.27	2.43	2.26	2.25	3.44	2.27	2.34	2.26	2.26	3.45	3.46	2.24	2.42	3.43	3.00	3.09	2.03	2.03
Lu	0.44	0.34	0.33	0.34	0.31	0.32	0.47	0.32	0.33	0.32	0.33	0.43	0.42	0.34	0.34	0.45	0.45	0.47	0.31	0.31
Hf	3.26	1.04	0.96	1.04	1.33	1.31	2.74	1.34	1.03	1.32	1.34	2.72	2.74	1.03	1.03	2.73	4.7	4.86	6.07	5.93
Ta	0.56	0.25	0.21	0.25	0.21	0.23	0.36	0.21	0.26	0.22	0.21	0.35	0.36	0.22	0.26	0.33	1.06	1.02	0.4	0.46
Pb	3.65	3.68	1.42	3.72	1.85	1.79	2.51	1.82	3.65	1.83	1.76	2.54	2.47	1.45	3.75	2.58	28.2	32.7	14.1	14.5
Th	1.75	0.52	0.35	0.48	0.52	0.54	1.56	0.52	0.53	0.49	0.55	1.54	1.61	0.33	0.51	1.53	11.5	13.9	11.2	11.4
U	0.53	0.12	0.08	0.11	0.12	0.09	0.36	0.11	0.13	0.12	0.12	0.35	0.34	0.09	0.09	0.33	1.96	2.19	0.90	0.99
(La/Yb)N	2.3	1.6	1.5	1.6	1.5	1.5	2.1	1.5	1.7	1.5	1.5	2.1	2.2	1.5	1.6	2.4				
δEu	0.9	1.1	1.1	1.0	1.1	1.1	0.9	1.1	1.1	1.1	1.1	0.9	0.9	1.1	1.0	0.9				

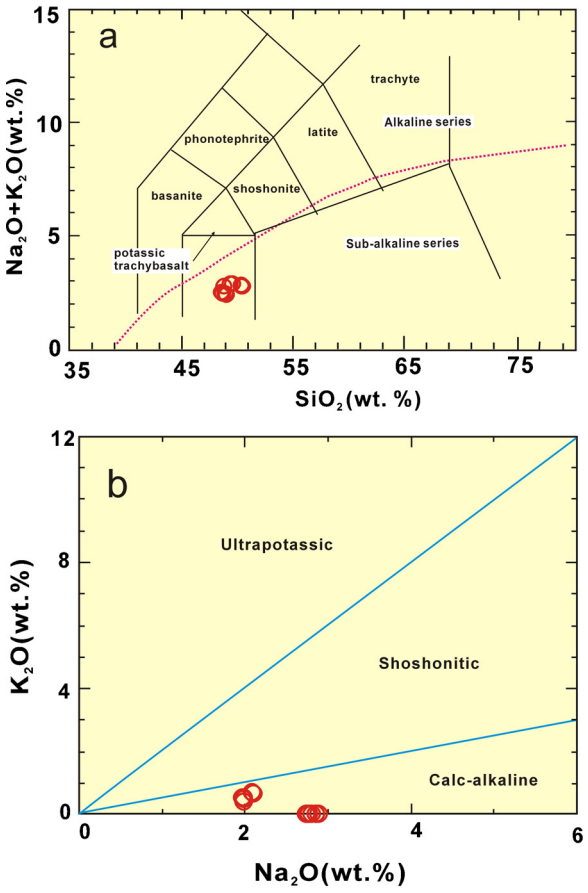

Fig. 4. Classification of mafic dykes from the NCC by: (a) TAS (after Middlemost, 1994; Le Maitre, 2002), using major element concentrations recalculated to 100% volatile-free compositions, and (b) K_2O vs. Na_2O (after Menzies and Kyle, 1972).

of which have significant LREE-enrichments and HREE-depletions but with different trace-element distribution patterns. The dykes are enriched in large ion lithophile elements (e.g. Pb and Ba), and Th-, U-, P-, and Ti-depleted in primitive mantle-normalized trace element diagrams, but have variable K enrichments and depletions, again consistent with their subdivision into two suites (Fig. 6b).

4.3. Sr–Nd and Pb isotopes

The Sr–Nd isotopic compositions of nine representative mafic dyke samples from the study area were determined (Table 4). These dykes have a small range of $(^{87}Sr/^{86}Sr)_i$ values (0.7025–0.7035) and positive $\varepsilon_{Nd}(t)$ values (5.6–5.8; Table 4 and Fig. 7) indicative of sourcing from a depleted region of the mantle. These Sr–Nd isotope compositions are different to those of other Paleoproterozoic and Neoproterozoic mafic dykes within the NCC within Shanxi and Gansu provinces (Liu et al., 2012a,b).

5. Discussion

5.1. Origin of the mafic dykes

New zircon, geochemical, and Sr–Nd isotope data presented in this study allow us to constrain the source, crustal contamination, fractional crystallization, and genetic model of this magmatic event in the NCC.

5.1.1. Mantle source

The mafic dykes contain low concentrations of SiO_2 (47.85–50.08 wt%; Table 2), suggesting that the magmas that formed these rocks were derived from an ultramafic (i.e. mantle) source, and not from melting of crustal material. An ultramafic source is also supported by the relatively high MgO (5.82–7.36 wt%) concentrations and elevated $Mg^{\#}$ values (42–54) of the mafic dykes. It is unlikely that crustal rocks were the source for these mafic magmas, as partial melting of any crustal material (e.g. Hirajima et al., 1990; Zhang et al., 1995; Kato et al., 1997) or lower crustal intermediate granulites in the deep crust (Gao et al., 1998a,b) would produce high-Si, low-Mg melts (i.e. granitoid liquids; Rapp et al., 2003). In addition, the studied dykes are characterized by special Zr/Nb (8.2–20), Th/La (0.07–0.15), Rb/Sr (0.03–0.16) and Sm/Nd (0.28–0.33) ratios (Table 3), suggesting that the mafic dykes were derived from the depleted lithospheric mantle source (Weaver, 1991). In addition to the above evidence, mafic dykes in the study area have low initial $^{87}Sr/^{86}Sr$ ratios (0.7025–0.7035) and positive but variable $\varepsilon_{Nd}(t)$ values (5.6–5.8; Table 4), consistent with a derivation from a depleted lithospheric mantle source.

5.1.2. Crustal contamination

Crustal contamination can lead to significant Sr–Nd isotope enrichments in basaltic rocks (Guo et al., 2004); however, the fact that dolerites within the study area are characterized by depleted Sr isotopic compositions (0.7025–0.7035) and positive $\varepsilon_{Nd}(t)$ values (5.6–5.8) suggests that the magmas that formed these dykes did not assimilate significant amounts of crustal material. In addition, crustal contamination would cause significant variation in Sr–Nd isotope compositions, positive correlations between MgO and $\varepsilon_{Nd}(t)$ values, and negative correlations between MgO and $(^{87}Sr/^{86}Sr)_i$ ratios, features that are absent from the dolerite samples analyzed during this study (Fig. 8). This is further supported by the presence of Th and U depletions relative to La in primitive mantle-normalized diagrams (Fig. 6b; Taylor and McLennan, 1985).

Moreover, the absence of inherited zircons suggests that the magmas that formed the mafic dykes in the study areas underwent negligible crustal contamination, indicating that these magmas were most likely derived from a depleted lithospheric mantle source.

5.1.3. Fractional crystallization

Mafic dykes from the Shangyaogou area have high $Mg^{\#}$ values (42–54; Table 2), consistent with significant crystal fractionation. Furthermore, the fact that MgO concentrations negatively correlate with SiO_2, TiO_2, Fe_2O_3, MnO, and P_2O_5 in all samples analyzed in this study (Fig. 5a, b, d, e and h) suggests that the magmas that formed these mafic dykes underwent fractionation of olivine, pyroxene, and Ti-bearing phases (rutile, ilmenite, and titanite) during the evolution of a more mafic parental magma. However, the absence of negative Eu anomalies in chondrite-normalized rare earth element (REE) diagrams is not indicative of plagioclase separation (Fig. 6a).

5.1.4. Genetic model

The fact that the presence of mafic dykes is indicative of lithospheric extension reveals that the NCC has undergone significant extensional tectonism. This suggests that knowledge of the origin of the mafic dykes analyzed during this study can further our understanding of Precambrian extensional faulting and tectonic evolution in this region, thus providing evidence for the evolution of the mantle beneath the NCC.

The interpretations outlined above indicate that the magmas that formed mafic dykes in the study area were not sourced from the melting of crustal material. However, all of the mafic dykes analyzed during this study have distinctive negative high field

Table 4
Sr–Nd isotopic compositions of mafic dykes within the northern NCC, using Chondrite Uniform Reservoir (CHUR) values, and decay constants of $\lambda_{Rb} = 1.42 \times 10^{-11}$ year^{-1} (Steiger and Jäger, 1977) and $\lambda_{Sm} = 6.54 \times 10^{-12}$ year^{-1} (Lugmair and Harti, 1978).

Sm (ppm)	Nd (ppm)	Rb (ppm)	Sr (ppm)	$^{87}Rb/^{86}Sr$	$^{87}Sr/^{86}Sr$	2σ	$(^{87}Sr/^{86}Sr)_i$	$^{147}Sm/^{144}Nd$	$^{143}Nd/^{144}Nd$	2σ	$(^{143}Nd/^{144}Nd)_i$	$\varepsilon_{Nd}(t)$
5.40	17.4	18.2	141	0.3730	0.712206	10	0.703520	0.1876	0.512838	8	0.510839	5.8
2.38	8.03	7.82	144	0.1569	0.706170	12	0.702515	0.1792	0.512746	9	0.510836	5.8
2.43	8.05	7.82	147	0.1537	0.706113	10	0.702533	0.1825	0.512778	10	0.510833	5.7
2.55	7.63	15.3	175	0.2527	0.708418	10	0.702535	0.2020	0.512987	9	0.510834	5.7
4.85	16.3	12.5	143	0.2526	0.708415	8	0.702533	0.1799	0.512746	10	0.510829	5.6
2.65	8.63	15.2	185	0.2374	0.708062	12	0.702533	0.1856	0.512805	9	0.510827	5.6
2.64	8.62	15.4	182	0.2445	0.708228	10	0.702534	0.1851	0.512803	10	0.510830	5.6
1.65	17.8	13.3	145	0.2651	0.708698	12	0.702526	0.0560	0.511424	8	0.510833	5.6
1.14	19.60	7.84	143	0.1584	0.706225	10	0.702536	0.0352	0.511201	10	0.510848	5.6

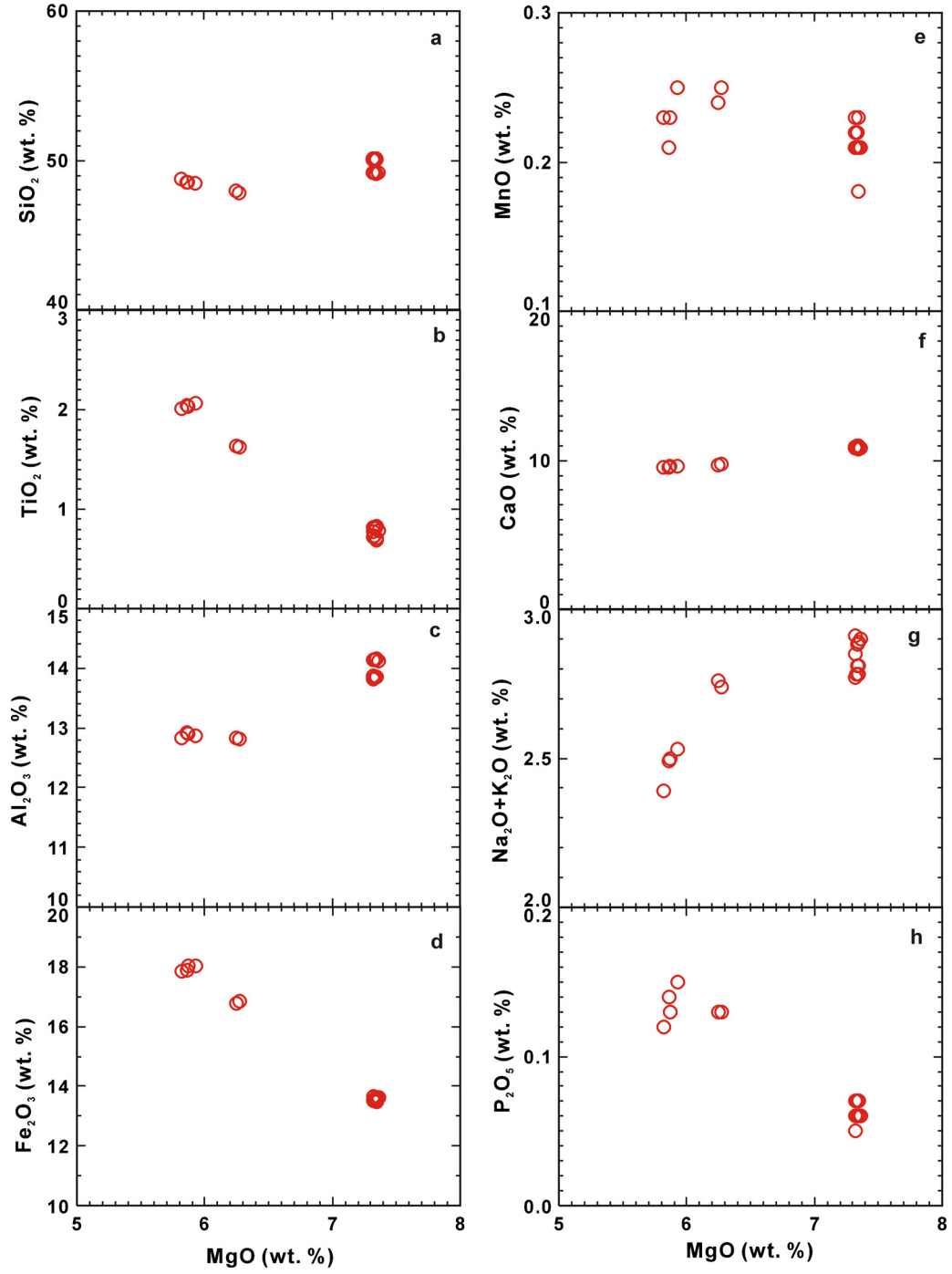

Fig. 5. Variations in major element concentrations compared with MgO (wt%) for mafic dykes of the northern NCC, China.

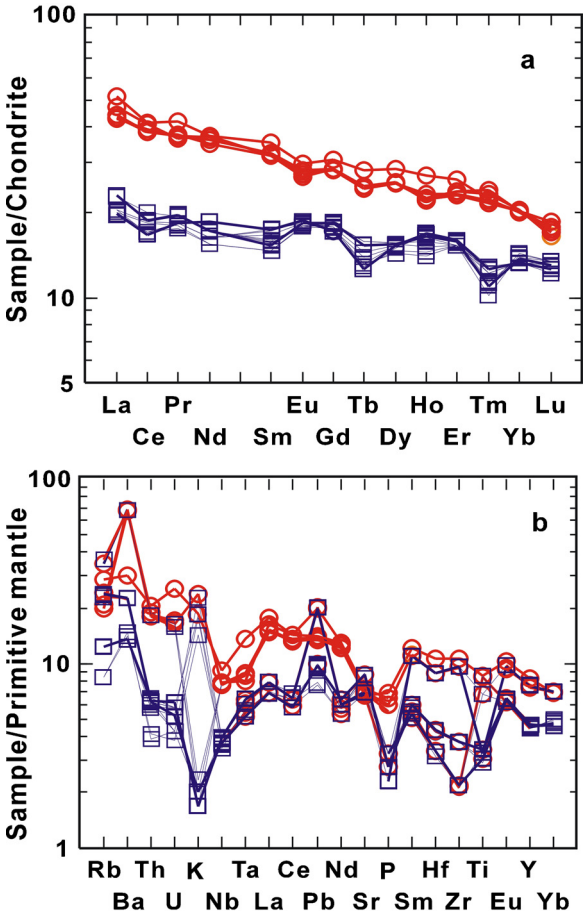

Fig. 6. (a) Chondrite-normalized REE and (b) primitive mantle-normalized incompatible element distribution diagrams for mafic dykes of the northern NCC, China; concentrations are normalized to chondrite and to primitive mantle values of Sun and McDonough (1989).

strength element (HFSE) anomalies (P and Ti), and positive Pb anomalies in primitive mantle-normalized diagrams (Fig. 6b). HFSE depletions are indicative of magmas that have incorporated proto-Tethyan oceanic or ancient continental crustal components (Zhang et al., 2005). In addition, the higher Ba/Nb ratios (31.8–87.5) of these rocks are significantly different from the majority of intraplate volcanic rocks, including N-MORB, OIB, alkali basalts,

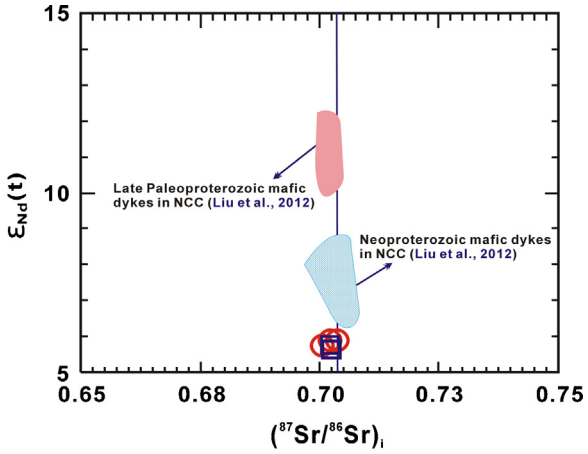

Fig. 7. Variations in initial $^{87}Sr/^{86}Sr$ vs. $\varepsilon_{Nd}(t)$ values for mafic dykes of the northern NCC, China; the field delineates the composition of Proterozoic mafic dykes within the NCC (Liu et al., 2012a,b). The NCC mafic dykes analyzed during this study plot within the depleted mantle source field.

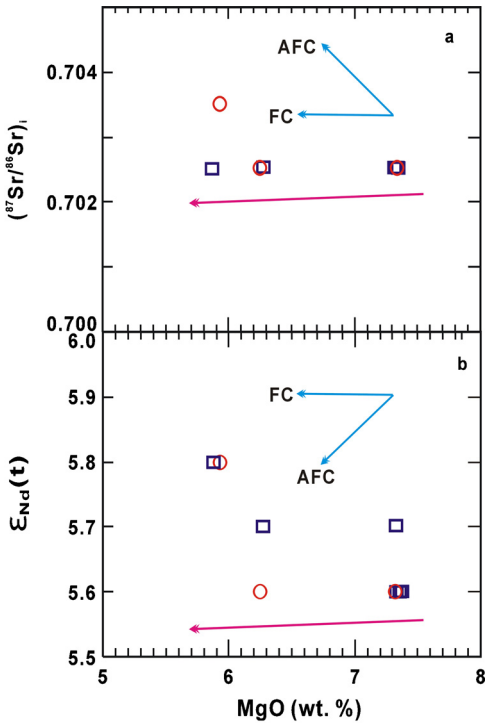

Fig. 8. Variations in: (a) initial $^{87}Sr/^{86}Sr$ ratios and (b) $\varepsilon_{Nd}(t)$ values with changing MgO concentrations for mafic dykes of the northern NCC, China.

and kimberlites, which have much lower Ba/Nb ratios (1–20; Jahn et al., 1999). These data may indicate that the mantle-derived magmas assimilated continental material (granitoids, granulites, or sediments) at some point prior to emplacement, most probably in the source region for the magmas. Nevertheless, it is necessary to know how these crustal materials were incorporated into the lithospheric mantle.

A possible model for the formation of these mafic dykes involves the foundering of the lower continental crust into an underlying region of the convecting mantle. This model is also thought to be a key process in plume magmatism, crustal evolution, and the formation of chemical heterogeneities within the mantle (Arndt and Goldstein, 1989; Kay and Kay, 1991; Rudnick and Fountain, 1995; Jull and Kelemen, 2001; Escrig et al., 2004; Gao et al., 2004, 2008; Elkins-Tanton, 2005; Lustrino, 2005; Anderson, 2006) associated with the unique chemical and physical properties of eclogites that are formed during high- to ultrahigh-pressure metamorphism of basalt. The fact that eclogite has a higher density than the surrounding lithospheric mantle peridotite (Rudnick and Fountain, 1995; Jull and Kelemen, 2001; Anderson, 2006; Levander et al., 2006) means that it can be recycled into the mantle (Arndt and Goldstein, 1989; Kay and Kay, 1991; Jull and Kelemen, 2001; Gao et al., 2004). However, eclogites also have lower melting temperatures than mantle peridotites (Yaxley and Green, 1998; Rapp et al., 1999; Yaxley, 2000; Kogiso et al., 2003; Sobolev et al., 2005, 2007), meaning that heating of silica-saturated eclogites during foundering will produce melts with silicic tonalite to trondhjemite compositions that can variably hybridize with the overlying mantle peridotite. These reactions can produce olivine-free pyroxenites, which, if subsequently melted, will generate basaltic magmas (Kogiso et al., 2003; Sobolev et al., 2005, 2007; Herzberg et al., 2007; Gao et al., 2008). As such, this model can explain both the metasomatism of the mantle and the origin of the primary magmas for the mafic dykes occurring throughout the NCC. Moreover, this model has been successfully used to explain the origin of Mesozoic mafic dykes within Shandong Province, China (Liu et al., 2008a,b, 2009).

5.2. Tectonic implications

Lithospheric extension has been demonstrated based upon the aforementioned interpretations. Accordingly, the study of mafic dykes and mafic dyke swarms can provide valuable information concerning the timing and various stages of extensional tectonics. Nevertheless, previous investigations have focused only on Mesozoic and Cenozoic mafic dykes from the NCC, and little attention has been paid to earlier episodes of lithosphere extension within the NCC, including those that formed in the Precambrian (2.5–0.6 Ga; Chen and Shi, 1983, 1994; Chen et al., 1992; Zhang and Sun, 2002; Shao and Zhang, 2002; Peng et al., 2005, 2007, 2008, 2010, 2011a,b; Hou et al., 2006; Yan et al., 2007; Li et al., 2010; Peng, 2010).

Current interpretations of extension-related igneous activity within the NCC, which are based upon the study of mafic dyke swarms, alkaline igneous rocks and the occurrence of suites of bimodal volcanic rocks, have indicated that there could have potentially been three periods of lithosphere extension during Proterozoic times. However, controversy has long surrounded the issue of whether there was any extensional activity that had occurred between 1.7 Ga and 1.6 Ga (Shao and Zhang, 2002; Yan et al., 2007). The precise ages determined in this study provide a support for the lithospheric extension at ~1.62 Ga. Hence, based upon the preliminary studies coupled with our data, we concur that there were three episodes of lithospheric extension affecting the NCC during Proterozoic time (i.e. 1.8–1.6 Ga, 1.3–1.2 Ga, and 0.8–0.7 Ga).

For the geological setting of the lithosphere extension, based upon the genetic model presented above, the foundering of lower crust may play an important role in lithosphere extension. For example, it is generally accepted that the Columbia super-continent formed between 2.1 Ga and 1.8 Ga (Condie, 2002; Zhao et al., 2002), and that during 1.8–1.3 Ga, continent extension occurred (Rogers and Santosh, 2002; Zhao et al., 2002; Lu et al., 2002; Ren et al., 2006). The first episode of Proterozoic lithosphere extension affecting the NCC (1.8–1.6 Ga) is consistent with the early stages of extension that culminated in the breakup of the Columbia super-continent (Zhao et al., 2003, 2011; Yan et al., 2007). If this is correct, this implies a possible relationship between extensional tectonics in both the NCC and Columbia super-continent. Nevertheless, based on the geochemical features and genetic model discussion, we propose that the foundering of lower crust has played an important role in the lithosphere extension.

6. Conclusions

Geochronological, geochemical, and Sr–Nd isotopic data presented here allow the following conclusions to be reached:

1. Zircon LA–ICP-MS U–Pb dating indicates that mafic dykes within the northern NCC in Shanxi Province formed between 1621 ± 6 and 1621 ± 7 Ma, indicating a Late Paleoproterozoic magmatic event.
2. The mafic dykes in the study area have sub-alkaline and calc-alkaline affinities. They have low and variable LREE concentrations [$(La/Yb)_N = 1.5–2.4$], with no Eu anomalies ($\delta Eu = 0.9–1.1$), positive Ba and Pb anomalies, negative T, U and HFSE (P and Ti) anomalies, and variable K anomalies. The dykes contain relatively low amounts of radiogenic Sr, as shown by $(^{87}Sr/^{86}Sr)_i$ values (0.7025–0.7035), and have high $\varepsilon_{Nd}(t)$ values (5.6–5.8), suggesting a derivation from a depleted region of the mantle that was hybridized during the foundering of lower crustal material.
3. The dykes were derived from a mantle source. The parental magmas of these dykes probably formed from fractional crystallization of a basaltic magma. The fractionation of olivine, pyroxene, hornblende, and Fe–Ti oxides (e.g. rutile, ilmenite, and titanite) occurred during ascent of these magmas, but with negligible crustal contamination.

Acknowledgements

This research was supported by the Opening Project (201206) of the State Key Laboratory of Ore deposit Geochemistry, Chinese Academia of Sciences, and National Natural Science Foundation of China (41373028). The authors thank Lian Zhou for assistance during Sr–Nd-Pb isotope analysis and Zhaochu Hu for assistance during LA–ICP-MS zircon U–Pb dating.

References

Andersen, T., 2002. Correction of common lead in U–Pb analyses that do not report ^{204}Pb. Chemical Geology 192, 59–79.
Anderson, D.A., 2006. Speculations on the nature and cause of mantle heterogeneity. Tectonophysics 146, 7–22.
Arndt, N.T., Goldstein, S.L., 1989. An open boundary between lower continental crust and mantle: its role in crust formation and crustal recycling. Tectonophysics 161, 201–212.
Chen, X.D., Shi, L.B., 1983. Primary research on the diabase dyke swarms in Wutai-Taihang area. Chinese Science Bulletin 16, 1002–1005.
Chen, X.D., Shi, L.B., 1994. Basic dyke swarms in extensional structures. In: Qian, X.L. (Ed.), Extensional Structures. Geological Publishing House, Beijing, pp. 71–74.
Chen, X.D., Shi, L.B., Jia, S.F., 1992. Proterozoic basic dyke swarms in North China. Seismology and Geology 14, 351–357 (in Chinese with English abstract).
Condie, K.C., 2002. Breakup of a paleoproterozoic super-continent. Gondwana Research 5, 41–43.
Elkins-Tanton, L.T., 2005. Continental magmatism caused by lithospheric delamination. In: Foulger, G.R., Natland, J.H., Presnall, D.C., Anderson, D.L. (Eds.), Plates, Plumes, and Paradigms, Geological Society of America. , pp. 449–462, Special Paper 388.
Escrig, S., Capmas, F., Dupré, B., Allégre, C.J., 2004. Osmium isotopic constraints on the nature of the DUPAL anomaly from Indian mid-ocean-ridge basalts. Nature 431, 59–63.
Féraud, G., Giannerini, G., Campredon, R., 1987. Dyke swarms as paleostress indicators in areas adjacent to continental collision zones: examples from the European and Northwest Arabian Plates. In: Halls, H.C., Fahrig, W.F. (Eds.), Mafic Dyke Swarms, 34, pp. 273–278, Geological Association of Canada Special Paper.
Gao, S., Luo, T.-C., Zhang, B.-R., Zhang, H.-F., Han, Y.-W., Zhao, Z.-D., Hu, Y.-K., 1998a. Chemical composition of the continental crust as revealed by studies in East China. Geochimica et Cosmochimica Acta 62, 1959–1975.
Gao, S., Rudnick, R., Yuan, H.L., Liu, X.M., Liu, Y.S., Xu, W.L., Ling, W.L., Ayers, J., Wang, X.C., Wang, Q.H., 2004. Recycling lower continental crust in the north China craton. Nature 432, 892–897.
Gao, S., Rudnick, R.L., Xu, W.L., Yuan, H.L., Liu, Y.S., Walker, R.J., Puchtel, I., Liu, X.M., Huang, H., Wang, X.R., Yang, J., 2008. Recycling deep cratonic lithosphere and generation of intraplate magmatism in the North China Craton. Earth and Planetary Science Letters 270, 41–53.
Gao, S., Zhang, B.-R., Jin, Z.-M., Kern, H., Luo, T.-C., Zhao, Z.-D., 1998b. How mafic is the lower continental crust? Earth and Planetary Science Letters 106, 101–117.
Gudmunsson, A., 1995. Infrastructure and mechanics of volcanic systems in Iceland. Journal of Volcanology and Geothermal Research 64, 1–22.
Guo, F., Fan, W.M., Wang, Y.J., Zhang, M., 2004. Origin of early Cretaceous calc-alkaline lamprophyres from the Sulu orogen in eastern China: implications for enrichment processes beneath continental collisional belt. Lithos 78, 291–305.
Guo, J.-H., Sun, M., Chen, F.-K., Zhai, M.-G., 2005. Sm–Nd and SHRIMP U–Pb zircon geochronology of high-pressure granulites in the Sanggan area, North China Craton: timing of Palaeoproterozoic continental collision. Journal of Asian Earth Sciences 24, 629–642.
Halls, H.C., 1982. The importance and potential of mafic dyke swarms in studies of geodynamic process. Geosciences Canada 9, 145–154.
Halls, H.C., Fahrig, W.F., 1987. Mafic dyke swarms. Geological Association of Canada. Special Paper 34, 1–503.
Herzberg, C., Asimow, P.D., Arndt, N., Niu, Y., Lesher, C.M., Fitton, J.G., Cheadle, M.J., Saunders, A.D., 2007. Temperatures in ambient mantle and plumes: Constraints from basalts, picrites, and komatiites. Geochemistry Geophysics Geosystems 8, 1525–2027.
Hirajima, T., Ishiwatari, A., Cong, B., Zhang, R., Banno, S., Nozaka, T., 1990. Coesite from Mengzhong eclogite at Donghai county, northern Jiangsu province, China. Mineralogy Magazine 54, 579–583.
Hou, G.T., Liu, Y.L., Li, J.H., 2006. Evidence for 1.8 Ga extension of the Eastern Block of the North China Craton from SHRIMP U–Pb dating of mafic dyke swarms in Shandong Province. Journal of Asian Earth Sciences 27, 392–401.
Huang, Z.X., Li, H.Y., Zheng, Y.J., Peng, Y.J., 2009. The lithosphere of North China Craton from surface wave tomography. Earth and Planetary Science Letters 288, 164–173.
Jahn, B.M., Wu, F.Y., Lo, C.H., Tsai, C.H., 1999. Crust mantle interaction induced by deep subduction of the continental crust: geochemical and Sr–Nd isotopic

evidence from post-collisional mafic–ultramafic intrusions of the northern Dabie complex, central China. Chemical Geology 157, 119–146.
John, D.A.P., Zhang, J.S., Huang, B.C., Andrew, P.R., 2010. Palaeomagnetism of Precambrian dyke swarms in the North China Shield: the 1.8 Ga LIP event and crustal consolidation in late Palaeoproterozoic times. Journal of Asian Earth Sciences 41, 504–524.
Jull, M., Kelemen, P.B., 2001. On the conditions for lower crustal convective instability. Journal of Geophysical Research 106, 423–446.
Kato, T., Enami, A., Zhai, M., 1997. Ultrahigh-pressure marble and eclogite in the Su–Lu ultrahigh-pressure terrane, eastern China. Journal of Metamorphic Geology 15, 169–182.
Kay, R.W., Kay, S.M., 1991. Creation and destruction of lower continental crust. Geologische Rundschau 80, 259–278.
Kogiso, T., Hirschmann, M.M., Frost, D.J., 2003. High-pressure partial melting of garnet pyroxenite: possible mafic lithologies in the source of ocean island basalts. Earth and Planetary Science Letters 216, 603–617.
Le Maitre, R.W., 2002. Igneous Rocks: A Classification and Glossary of Terms, 2nd ed. Cambridge University Press, Cambridge, pp. 236.
Levander, A., Niu, F., Lee, C.T.A., Cheng, X., 2006. Imaging the continental lithosphere. Tectonophysics 416, 167–185.
Li, S.Z., Zhao, G.C., 2007. SHRIMP U–Pb zircon geochronology of the Liaoji granitoids: constraints on the evolution of the Paleoproterozoic Jiao-Liao-Ji belt in the Eastern Block of the North China Craton. Precambrian Research 158, 1–16.
Li, S.Z., Zhao, G.C., Sun, M., Han, Z.Z., Zhao, G.T., Hao, D.F., 2006. Are the South and North Liaohe Groups of the North China Craton different exotic terranes? Nd isotope constraints. Gondwana Research 9, 198–208.
Li, X.P., Yang, Z.Y., Zhao, G.C., Grapes, R., Guo, J.H., 2011. Geochronology of khondalite-series rocks of the Jining Complex: confirmation of depositional age and tectonometamorphic evolution of the North China craton. International Geology Review 53, 1194–1211.
Li, T.S., Zhai, M.G., Peng, P., Chen, L., Guo, J.H., 2010. 2.5 billion year old coeval ultramafic–mafic and syenitic dykes in Eastern Hebei: implications for cratonization of the North China Craton. Precambrian Research 180, 143–155.
Lin, G., Zhao, C.B., Xiao, H.Q., Chen, G.H., Yan, Y., Zhang, D.S., Liu, S.L., Chen, Y.P., 2008a. Dynamic mechanisms and models of tectonic activiztion in north China Craon. Geotectonica et Metallogenia 32, 133–142 (in Chinese with English abstract).
Lin, W., Faure, M., Monié, P., Schärer, U., Panis, D., 2008b. Mesozoic extensional tectonics in Eastern Asia: the south Liaodong peninsula metamorphic core complex (NE China). The Journal of Geology 116, 134–154.
Liu, D.Y., Nutman, A.P., Compston, W., Wu, J.S., Shen, Q.H., 1992. Remnants of 3800 Ma crust in the Chinese part of the Sino-Korean craton. Geology 20, 339–342.
Liu, S., Hu, R.Z., Feng, G.Y., Yang, Y.H., Feng, C.X., Qi, Y.Q., Wang, T., 2010a. Distribution and significance of the mafic dykes swarms since Mesozoic in North China Craton. Geological Bulletin of China 29, 259–267 (in Chinese with English abstract).
Liu, S., Hu, R., Gao, S., Feng, C., Coulson, I.M., Feng, G., Qi, Y., Yang, Y., Yang, C., Tang, L., 2012b. U–Pb zircon age, geochemical and Sr–Nd isotopic data as constraints on the petrogenesis and emplacement time of the Precambrian mafic dyke swarms in the North China Craton (NCC). Lithos 140–141, 38–52.
Liu, S., Hu, R., Gao, S., Feng, C., Coulson, I.M., Feng, G., Qi, Y., Yang, Y., Yang, C., Tang, L., 2013. Zircon U–Pb age and Sr–Nd–Hf isotopic constraints on the age and origin of Triassic mafic dykes, Dalian area, Northeast China. International Geology Review 55, 249–262.
Liu, S., Hu, R.-Z., Gao, S., Feng, C.-X., Qi, L., Zhong, H., Xiao, T., Qi, Y.-Q., Wang, T., Coulson, I.M., 2008a. Zircon U–Pb geochronology and major, trace elemental and Sr–Nd–Pb isotopic geochemistry of mafic dykes in western Shandong Province, east China: constrains on their petrogenesis and geodynamic significance. Chemical Geology 255, 329–345.
Liu, S., Hu, R., Gao, S., Feng, C., Feng, G., Qi, Y., Coulson, I.M., Yang, Y., Yang, C., Tang, L., 2012a. Geochemical and isotopic constraints on the age and origin of mafic dykes from eastern Shandong Province, eastern North China Craton. International Geology Review 54, 1389–1400.
Liu, S., Hu, R., Gao, S., Feng, C., Qi, Y., Wang, T., Feng, G., Coulson, I.M., 2008b. U–Pb zircon age, geochemical and Sr–Nd–Pb–Hf isotopic constraints on age and origin of alkaline intrusions and associated mafic dykes from Sulu orogenic belt, Eastern China. Lithos 106, 365–379.
Liu, S., Hu, R., Gao, S., Feng, C., Yu, B., Feng, G., Qi, Y., Wang, T., Coulson, I.M., 2009. Petrogenesis of Late Mesozoic mafic dykes in the Jiaodong Peninsula, eastern North China Craton and implications for the foundering of lower crust. Lithos 113, 621–639.
Liu, S., Hu, R.Z., Zhao, J.H., Feng, C.X., Zhong, H., Cao, J.J., Shi, D.N., 2005. Geochemical characteristics and petrogenetic investigation of the late Mesozoic lamprophyres of Jiaobei, Shandong Province. Acta Petrologica Sinica 21, 947–958 (in Chinese with English abstract).
Liu, S., Zou, H.B., Hu, R.Z., Zhao, J.H., Feng, C.X., 2006. Mesozoic mafic dykes from the Shandong Peninsula, North China Craton: petrogenesis and tectonic implications. Geochemical Journal 40, 181–195.
Liu, Y.S., Hu, Z.C., Zong, K.Q., Gao, C.G., Gao, S., Xu, J., Chen, H.H., 2010b. Reappraisement and refinement of zircon U–Pb isotope and trace element analyses by LA–ICP–MS. Chinese Science Bulletin 55, 1535–1546.
Lu, S.N., Yang, C.L., Li, H.K., 2002. North China continent and Columbia supercontinent. Earth Science Frontiers 9, 223–233 (in Chinese with English abstract).
Lu, S.N., Zhao, G.C., Wang, H.C., Hao, G.J., 2008. Precambrian metamorphic basement and sedimentary cover of the North China Craton: review. Precambrian Research 160, 77–93.
Ludwig, K.R., 2003. User's manual for Isoplot/Ex. Version 3. 00. A Geochronological Toolkit for Microsoft Excel, vol. 4. Berkeley Geochronology Center Special Publication, pp. 1–70.
Lugmair, G.W., Harti, K., 1978. Lunar initial $^{143}Nd/^{144}Nd$: differential evolution of the lunar crust and mantle. Earth and Planetary Science Letters 39, 349–357.
Luo, Y., Sun, M., Zhao, G.C., Ayers, J.C., Li, S.Z., Xia, X.P., Zhang, J.H., 2008. A comparison of U–Pb and Hf isotopic compositions of detrital zircons from the North and South Liaohe Group: constraints on the evolution of the Jiao-Liao-Ji Belt, North China Craton. Precambrian Research 163, 279–306.
Lustrino, M., 2005. How the delamination and detachment of lower crust can influence basaltic magmatism. Earth-Science Reviews 72, 21–38.
Menzies, M.A., Kyle, P.R., 1972. Continental volcanism: a crust–mantle probe. In: Menzies, M.A. (Ed.), Continental Mantle. Oxford University Press, Oxford, pp. 157–177.
Middlemost, E.A.K., 1994. Naming materials in the magma/igneous rock system. Earth-Science Reviews 74, 193–227.
Peng, P., 2010. Reconstruction and Interpretation of Giant Mafic Dyke Swarms: A Case Study of 1.78 Ga Magmatism in the North China Craton. Geological Society, London, pp. 163–178, Geological Society Special Publication, 338.
Peng, P., Bleeker, W., Ernst, R.E., Söderlund, U., McNicoll, V., 2011a. U–Pb baddeleyite ages, distribution and geochemistry of 925 Ma mafic dykes and 900 Ma sills in the North China craton: evidence for a Neoproterozoic mantle plume. Lithos 127, 210–221.
Peng, P., Guo, J.H., Zhai, M.G., Bleeker, W., 2010. Paleoproterozoic gabbronoritic and granitic magmatism in the northern margin of the North China craton: evidence of crust–mantle interaction. Precambrian Research 183, 635–659.
Peng, P., Zhai, M.G., Guo, J.H., Kusky, T., Zhao, T.P., 2007. Nature of mantle source contributions and crystal differentiation in the petrogenesis of the 1.78 Ga mafic dykes in the central North China craton. Gondwana Research 12, 29–46.
Peng, P., Zhai, M.G., Li, Q.L., Wu, F.Y., Hou, Q.L., Li, Z., Li, T.S., Zhang, Y.B., 2011b. Neoproterozoic (900 Ma) Sariwon sills in North Korea: geochronology, geochemistry and implications for the evolution of the south-eastern margin of the North China Craton. Gondwana Research 20, 243–254.
Peng, P., Zhai, M.-G., Li, Z., Wu, F.-Y., Hou, Q.-L., 2008. Neoproterozoic (~820 Ma) mafic dyke swarms in the North China Craton: implication for a conjoint to the Rodinia supercontinent? In: 13th Gondwana Conference, Dali, China, pp. 160–161, Abstracts.
Peng, P., Zhai, M.-G., Zhang, H.-F., Guo, J.-H., 2005. Geochronological constraints on the Palaeoproterozoic evolution of the North China Craton: SHRIMP zircon ages of different types of mafic dykes. International Geology Review 47, 492–508.
Potts, P.J., Kane, J.S., 2005. International association of geoanalysts certificate of analysis: certified reference material OU-6 (Penrhyn slate). Geostandards and Geoanalytical Research 29, 233–236.
Qi, L., Hu, J., Grégoire, D.C., 2000. Determination of trace elements in granites by inductively coupled plasma mass spectrometry. Talanta 51, 507–513.
Rapp, R.P., Shimizu, N., Norman, M.D., 2003. Growth of early continental crust by partial melting of eclogite. Nature 425, 605–609.
Rapp, R.P., Shimizu, N., Norman, M.D., Applegate, G.S., 1999. Reaction between slab-derived melts and peridotite in the mantle wedge: experimental constraints at 3.8-GPa. Chemical Geology 160, 335–356.
Ren, K.X., Yan, G.H., Cai, J.H., 2006. Chronology and geological implication of the Paleo-Mesoproterozoic alkaline-rich intrusions belt from the northern part in North China Craton. Acta Petrologica Sinica 22, 377–386 (in Chinese with English abstract).
Rogers, J., Santosh, M., 2002. Configuration of Columbia, a Mesoproterozoic supercontinent. Gondwana Research 5, 5–22.
Rudnick, R.L., Fountain, D.M., 1995. Nature and composition of the continental crust: a lower crustal perspective. Reviews of Geophysics 33, 267–309.
Shao, J.A., Zhang, L.Q., 2002. Mesozoic dyke swarms in the north of North China. Acta Petrologica Sinica 18, 312–318 (in Chinese with English abstract).
Shao, J.A., Zhang, Y.B., Zhang, L.Q., Mu, B.L., Wang, P.Y., Guo, F., 2003. Early Mesozoic dyke swarms of carbonatites and lamprophyres in Datong area. Acta Petrologica Sinica 19, 93–104.
Sobolev, A.V., Hofmann, A.W., Kuzmin, D.V., Yaxley, G.M., Arndt, N.T., Chung, S.L., Danyushevsky, L.V., Elliott, T., Frey, F.A., Garcia, M.O., Gurenko, A.A., Kamenetsky, V.S., Kerr, A.C., Krivolutskaya, N.A., Matvienkov, V.V., Nikogosian, I.K., Rocholl, A., Sigurdsson, I.A., Sushchevskaya, N.M., Teklay, M., 2007. The amount of recycled crust in sources of mantle-derived melts. Science 316, 412–417.
Sobolev, A.V., Hofmann, A.W., Sobolev, S.V., Nikogosian, I.K., 2005. An olivine-free mantle source of Hawaiian shield basalts. Nature 434, 590–597.
Steiger, R.H., Jäger, E., 1977. Subcommission on geochronology; convention on the use of decay constants in geochronology and cosmochronology. Earth and Planetary Science Letters 36, 359–362.
Sun, S.S., McDonough, W.F., 1989. Chemical and isotopic systematics of oceanic basalts: implications for mantle composition and processes. In: Saunders, A.D., Norry, M.J. (Eds.), Magmatism in the Ocean Basins. Geological Society Special Publication, London, pp. 313–345.
Tam, P.Y., Zhao, G.C., Liu, F.L., Zhou, X.W., Sun, M., Li, S.Z., 2011. SHRIMP U–Pb zircon ages of high-pressure mafic and pelitic granulites and associated rocks in the Jiaobei massif: constraints on the metamorphic ages of the Paleoproterozoic Jiao-Liao-Ji Belt in the North China Craton. Gondwana Research 19, 150–162.

Tam, P.Y., Zhao, G.C., Sun, M., Li, S.Z., Wu, M.L., Yin, C.Q., 2012b. Petrology and metamorphic P–T path of high-pressure mafic granulites from the Jiaobei massif in the Jiao-Liao-Ji Belt, North China Craton. Lithos 155, 94–109.
Tam, P.Y., Zhao, G.C., Zhou, X.W., Sun, M., Li, S.Z., Yin, C.Q., Wu, M.L., He, Y.H., 2012a. Metamorphic P–T path and implications of high-pressure pelitic granulites from the Jiaobei massif in the Jiao-Liao-Ji Belt, North China Craton. Gondwana Research 22, 104–117.
Tarney, J., Weaver, B.L., 1987. Geochemistry and petrogenesis of early Proterozoic dyke swarms. In: Halls, H.C., Fahrig, W.C. (Eds.), Mafic Dyke Swarms, vol. 34, pp. 81–93, Special Publication-Geological Association of Canada.
Taylor, S.R., McLennan, S.M., 1985. The Continental Crust: Its Composition and Evolution. An Examination of the Geochemical Record Preserved in Sedimentary Rocks. Blackwell, Oxford London Press, pp. 312.
Thompson, M., Potts, P.J., Kane, J.S., Wilson, S., 2000. An international proficiency test for analytical geochemistry laboratories—report on Round, 5, August 1999. Geostandards and Geoanalytical Research 24, E1–E28.
Wang, F., Li, X.P., Chu, H., Zhao, G.C., 2011. Petrology and metamorphism of khondalites from Jining Complex in the North China Craton. International Geology Review 53, 212–229.
Wang, T., Zheng, Y.D., Zhang, J.J., Wang, X.S., Zeng, L.S., Tong, Y., 2007. Some problems in the study of Mesozoic extensional structure in the North China Craton and its significance for the study of lithospheric thinning. Geological Bulletin of China 26, 1154–1166 (in Chinese with English abstract).
Wang, Y.J., Zhang, Y.Z., Zhao, G.C., Fan, W.M., Xia, X.P., Zhang, F.F., Zhang, A.M., 2009. Zircon U–Pb geochronological and geochemical constraints on the petrogenesis of the Taishan sanukitoids (Shanddong): Implications for Neoarchean subduction in the eastern block, North China Craton. Precambrian Research 174, 273–286.
Wang, Y.M., Gao, Y.S., Han, H.M., Wang, X.H., 2003. Practical Handbook of Reference Materials for Geoanalysis. Geological Publishing House, Beijing (in Chinese).
Weaver, B.I., 1991. The origin of ocean island end-member compositions: trace element and isotopic constraints. Earth and Planetary Science 104, 381–397.
Wilde, S.A., Zhao, G.-C., Sun, M., 2002. Development of the North China craton during the Late Archaean and its final amalgamation at 1.8 Ga: some speculation on its position within a global Palaeoproterozoic Supercontinent. Gondwana Research 5, 85–94.
Wu, F.Y., Xu, Y.G., Gao, S., Zheng, J.P., 2008. Lithospheric thinning and destruction of the North China Craton. Acta Petrologica Sinica 24, 1145–1174 (in Chinese with English abstract).
Wu, K.K., Zhao, G.C., Sun, M., Yin, C.Q., He, Y.H., Tam, P.Y., 2013a. Metamorphism of the northern Liaoning Complex: implications for the tectonic evolution of Neoarchean basement of the eastern block, North China Craton. Geoscience Frontiers 4, 305–320.
Wu, M.L., Zhao, G.C., Sun, M., Li, S.Z., He, Y.H., Bao, Z., 2013b. Zircon U–Pb geochronology and Hf isotopes of major lithologies from the Yishui Terrane: implications for the crustal evolution of the eastern block, North China Craton. Lithos 170–171, 164–178.
Xia, X.P., Sun, M., Zhao, G.C., Wu, F.Y., Xu, P., Zhang, J.S., 2008. Paleoproterozoic crustal growth events in the Western Block of the North China Craton: Evidence from detrital zircon Hf and whole rock Sr–Nd isotopes of the khondalites in the Jining Complex. American Journal of Science 308, 304–327.
Xu, Y.G., 2004. Lithospheric thinning beneath North China: a temporal and spatial perspective. Geological Journal of China Universities 10, 324–331 (in Chinese with English abstract).
Yan, G.H., Cai, J.H., Ren, K.X., He, G.Q., Mu, B.L., Xu, B.L., Li, F.T., Yang, B., 2007. Intraplate extensional magmatism of North China Craton and break-up of three supercontinents and their deep dynamics. Geological Journal of China Universities 13, 161–174 (in Chinese with English abstract).
Yang, J.H., Chung, S.L., Zhai, M.G., Zhou, X.H., 2004. Geochemical and Sr–Nd–Pb isotopic compositions of mafic dykes from the Jiaodong Peninsula, China: evidence for vein-plus-peridotite melting in the lithospheric mantle. Lithos 73, 156–160.
Yaxley, G.M., 2000. Experimental study of the phase and melting relations of homogeneous basalt plus peridotite mixtures and implications for the petrogenesis of flood basalts. Contributions to Mineralalogy and Petrology 139, 326–338.
Yaxley, G.M., Green, D.H., 1998. Reactions between eclogite and peridotite: mantle refertilisation by subduction of oceanic crust. Schweizerische Mineralogische und Petrographische Mitteilungen 78, 243–255.
Yin, C.Q., Zhao, G.C., Guo, J.H., Sun, M., Zhou, X.W., Zhang, J., Xia, X.P., Liu, C.H., 2011. U–Pb and Hf isotopic study of zircons of the Helanshan Complex: constraints on the evolution of the Khondalite Belt in the Western Block of the North China Craton. Lithos 122, 25–38.
Yin, C.Q., Zhao, G.C., Sun, M., Xia, X.P., Wei, C.J., Zhou, X.W., Leung, W.H., 2009. LA–ICP-MS U–Pb zircon ages of the Qianlishan Complex: constraints on the evolution of the Khondalite Belt in the Western Block of the North China Craton. Precambrian Research 174, 78–94.
Yuan, H.L., Gao, S., Liu, X.M., Li, H.M., Gunther, D., Wu, F.Y., 2004. Accurate U–Pb age and trace element determinations of zircon by laser ablation–inductively coupled plasma mass spectrometry. Geostandards Newsletter 28, 353–370.
Zhai, M.G., 2012. Evolution of the North China Craton and early plate tectonics. Acta Geologica Sinica 86, 1335–1349 (in Chinese with English abstract).
Zhai, M.G., Bian, A.G., 2000. Supercontinent flatten in late Neoarchean and the cracking during Paleoproterozoic and Mesoproterozoic of the NCC. Science in China 30, 129–137.
Zhai, M.G., Fang, H.R., Yang, J.H., Miao, L.C., 2004. Large-scale cluster of cold deposits in east Shandong: anorogenic metallogenesis. Earth Science Frontiers 11, 95–98 (in Chinese with English abstract).
Zhai, M.G., Zhu, R.X., Liu, J.M., Meng, Q.R., Hou, Q.L., Hu, S.B., Li, Z., Zhang, H.F., Liu, W., 2003. The critical time frame of turning pint of tectonic regime. Sciences in China (D) 33, 913–920.
Zhang, C.H., 2009. Selected tectonic topics in the investigation of geodynamic process of destruction of North China Craton. Earth Science Frontiers 16, 203–214 (in Chinese with English abstract).
Zhang, G.W., Meng, Q.R., Lai, S.C., 1995. Tectonics and structure of Qinling orogenic belt. Science in China 38, 1379–1394.
Zhang, H.F., Sun, M., 2002. Geochemistry of Mesozoic basalts and mafic dykes, southeastern north China Carton, and tectonic implications. International Geology Review 44, 370–382.
Zhang, H.F., Sun, M., Zhou, X.H., Ying, J.F., 2005. Geochemical constraints on the origin of Mesozoic alkaline intrusive complexes from the North China Craton and tectonic implications. Lithos 81, 297–317.
Zhao, G.C., 2009. Metamorphic evolution of major tectonic units in the basement of the North China Craton: key issues and discussion. Acta Petrologica Sinica 25, 1772–1792.
Zhao, G.C., Gawood, P.A., Li, S.Z., Wilde, S.A., Sun, M., Zhang, J., He, Y.H., Yin, C.Q., 2012. Amalgamation of the North China Craton: key issue and discussion. Precambrian Research 222–223, 55–76.
Zhao, G.C., Cawood, P.A., Wilde, S.A., 2002. Review of global 2.1–1.8 Ga orogens: implications for a pre-Rodinia supercontinent. Earth-Science Reviews 59, 125–162.
Zhao, G.C., Li, S.Z., Sun, M., Wilde, S.A., 2011. Assembly, accretion, and break-up of the Palaeo-Mesoproterozoic Columbia supercontinent: records in the North China Craton revisited. International Geology Review 53, 1331–1356.
Zhao, G.C., Sun, M., Wilde, S.A., Li, S.Z., 2003. Assembly, accretion and breakup of the Paleo-Mesoproterozoic Columbia supercontinent: records in the North China Craton. Gondwana Research 6, 417–434.
Zhao, G.C., Sun, M., Wilde, S.A., Li, S.-Z., 2005. Late Archaean to Palaeoproterozoic evolution of the North China Craton: key issues revisited. Precambrian Research 136, 177–202.
Zhao, G.C., Wilde, S.A., Cawood, P.A., Sun, M., 2001. Archean blocks and their boundaries in the North China Craton: lithological, geochemical, structural and P–T path constraints and tectonic evolution. Precambrian Research 107, 45–73.
Zhao, G.C., Wilde, S.A., Guo, J.H., Gawood, P.A., Sun, M., Li, X.P., 2010. Single zircon grains record two paleoproterozoic collisional events in the North China Craton. Precambrian Research 177, 266–276.
Zhao, G.C., Zhai, M.G., 2013. Lithotectonic elements of Precambrian basement in the North China Craton: review and tectonic implications. Gondwana Research 23, 1207–1240.
Zhao, J.X., McCulloch, M.T., 1993. Melting of a subduction-modified continental lithospheric mantle: evidence from late Proterozoic mafic dyke swarms in central Australia. Geology 21, 463–466.
Zheng, J.P., Griffin, W.L., O'Reilly, S.Y., Lu, F.X., Wang, C.Y., Zhang, M., FangZheng, W., Li, H.M., 2005. 3.6 Ga lower crust in central China: new evidence on the assembly of the North China Craton. Geology 32, 229–232.
Zhou, X.W., Zhao, G.C., Wei, C.J., Geng, Y.S., Sun, M., 2008. Metamorphic evolution and Th–U–Pb zircon and monazite geochronology of high-pressure pelitic granulites in the Jiaobei massif of the North China Craton. American Journal of Science 308, 328–350.